461

New experimental system for base-isolated structures with various dampers and limit aspect ratio

I. Takewaki[*], M. Kanamori, S. Yoshitomi[a] and M. Tsuji

Department of Architecture and Architectural Engineering,
Graduate School of Engineering, Kyoto University,
Kyotodaigaku-Katsura, Nishikyo-ku, Kyoto 615-8540, Japan

Abstract. A new experimental system of base-isolated structures is proposed. There are two kinds of dampers usually used in the base-isolated buildings, one is a viscous-type damper and the other is an elastic-plastic hysteretic-type damper. The base-isolated structure with a viscous damper and that with an elastic-plastic hysteretic damper are compared in this paper. The viscous damper is modeled by a mini piston and the elastic-plastic hysteretic damper is modeled by a low yield-point steel. The capacity of both dampers is determined so that the dissipated energies are equivalent at a specified deformation. When the capacity of both dampers is determined according to this criterion, it is shown that the response of the base-isolated structure with the elastic-plastic hysteretic damper is larger than that with the viscous damper. This characteristic is demonstrated through the comparison of the bound of the aspect ratio. It is shown that the bound of aspect ratio for the base-isolated structure with the elastic-plastic hysteretic damper is generally smaller than that with the viscous damper.

When the base-isolated structure is subjected to long-duration input, the mechanical property of the elastic-plastic hysteretic damper deteriorates and the response of the base-isolated structure including that damper becomes larger than that with the viscous damper. The effect of this change of material properties on the response of the base-isolated structure is also investigated.

Keywords: base-isolated structure; experiment; viscous and hysteretic dampers; aspect ratio; long-duration input; dissipation energy

1. Introduction

It is usually recognized (e.g., see Naeim and Kelly 1999) that base-isolation systems are very useful in reducing the acceleration and displacement responses relative to base of buildings caused by earthquakes. Base-isolation systems were introduced in many buildings and facilities after the Northridge earthquake (1994) and Hyogoken-Nambu earthquake (1995) (for example, Clemente and Buffarini 2010, Olmos and Roesset 2010, Nakamura *et al.* 2011a, b, Mahmoud and Jankowski, 2010, Nanda *et al.* 2012). It is believed that base-isolation systems are effective only for ground motions without long-period components because long-period ground motions induce unfavorable

---

resonant responses (Earthquake Spectra 1988, Kamae *et al.* 2004, Takewaki *et al.* 2011, 2013, Celebi *et al.* 2012, Minami *et al.* 2012). In fact, most of the ground motions recorded in the USA include high-frequency components in general (Newmark and Hall 1982, Abrahamson *et al.* 1998), and long-period ground motions have never been discussed except in a few cases, e.g. Landers in 1992 and Northridge in 1995 (Hall *et al.* 1995, Heaton *et al.* 1995, Zhang and Iwan 2002, Jangid and Kelly 2001). Even in these cases, the period range of the long-period wave components, so-called pulse waves, is rather short (2–3s) compared to those (5–10s) discussed in Japan (MLIT 2010, Takewaki *et al.* 2011, 2013).

Base-isolation systems are effective for low-rise stiff buildings and most of base-isolation systems have been installed in those buildings (Naeim and Kelly 1999, Hijikata *et al.* 2012). Some performance verification experiments have also been conducted so far (for example, Makris and Chang 2000, Madden *et al.* 2002, Sahasrabudhe and Nagarajaiah 2005). However, not a few tall base-isolated buildings are being planned and constructed in Japan (Ariga *et al.* 2006, Takewaki 2008, Takewaki and Fujita 2009 and Yamamoto *et al.* 2011). In this situation, it may be meaningful to discuss the response characteristics of base-isolated buildings in view of the bound of aspect ratio of tall base-isolated buildings and clarify the characteristics of such buildings. It is also desired to investigate the effect of the long-duration input on the change in mechanical properties of dampers (Jangid and Banerji 1998, Fujita and Takewaki 2011) and the effect of that change on the bound of aspect ratio.

The purpose of this paper is to propose a new experimental system of base-isolated structures with various dampers and disclose the limit of aspect ratios (Hino *et al.* 2008, Li and Wu 2006). The aspect ratio bounds are obtained by using the experimental results on the load-displacement relation (hysteresis loop) of the dampers and their simplified models in the analytical procedure. There are two kinds of dampers used usually in the base-isolated buildings, one is a viscous-type damper and the other is an elastic-plastic hysteretic-type damper. The base-isolated structure with a viscous damper and that with an elastic-plastic hysteretic damper are compared in this paper.   The innovative feature of this paper is to use the bound of aspect ratio as a measure of safety margin of tall base-isolated buildings. The introduction of a plot of the aspect ratio-base shear coefficient relation for a design condition together with the aspect ratio-response base shear coefficient relation under the design earthquake enables structural designers to understand the true safety margin in a unified manner. In a conventional procedure to check the satisfaction of the design conditions for a selected building with an aspect ratio, it may be difficult to understand the true safety margin for all the design constraints. The viscous damper is modeled by a mini piston and the elastic-plastic hysteretic damper is modeled by a low yield-point steel connected to two steel bars. In the elastic-plastic hysteretic damper, the bending deformation of a low yield-point steel bar is used. The capacity of both dampers is determined so that the dissipated energies are equivalent at a specified deformation. When the capacity of both dampers is determined according to this criterion, it is shown that the response of the base-isolated structure with the elastic-plastic hysteretic damper is larger than that with the viscous damper. This characteristic is demonstrated through the comparison of the bound of the aspect ratio (Hino *et al.* 2008, Li and Wu 2006). It is shown that the bound of aspect ratio for the base-isolated structure with the elastic-plastic hysteretic damper is smaller than that with the viscous damper.

When the base-isolated structure is subjected to a long-duration input, the mechanical property of the elastic-plastic hysteretic damper deteriorates and the response of the base-isolated structure
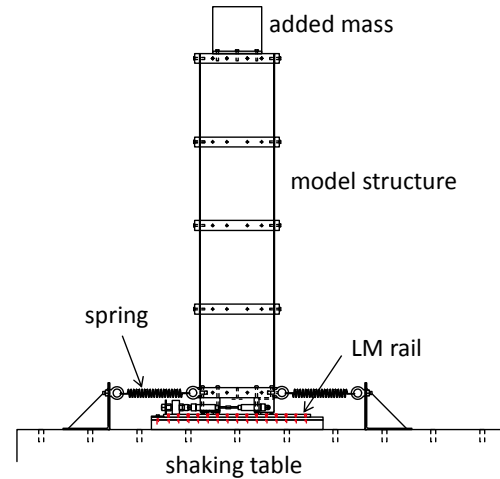
Photo 1 Four-story base-isolated test structure

Fig. 1 Side-view of test structure

becomes larger than that with the viscous damper. The effect of this change of material properties on the response of the base-isolated structure (Fujita and Takewaki 2011) is also investigated.

2. Design of test structures and dampers

2.1 Design of test structures

A four-story test structure is designed so that the fundamental natural period of the model with fixed base attains 0.53(s). The story stiffness is provided by four steel-plate springs shown in Photo 1 and Fig. 1. A test structure with eight steel-plate springs per story is also used so as to model a stiffer super structure. The test structure is put on two almost friction-free rails (static friction coefficient = 0.003) which are located on the shaking table (see Photo 1 and Fig. 1). The mass per floor except the roof is 2(kg) and the roof mass is 22(kg). The large mass was used to make the natural period of the base-isolated structure an acceptable one. The story stiffness of the structure with four steel-plate springs is constant throughout the stories and is 16.7(N/mm). The stiffness of the base-isolation story (without the stiffness of the elastic-plastic hysteretic damper) is 0.55(N/mm) and is represented by two springs installed as shown in Fig. 1. The fundamental natural period of the base-isolated model (four steel-plate springs) with a viscous damper is 1.69(s) and that of the model with a hysteretic damper is 0.883(s).

2.2 Design of dampers

A viscous damper is modeled by a mini piston and an elastic-plastic hysteretic damper is represented by a low yield-point steel which is usually called 'LY225'. While the mini piston is installed in parallel with the spring in the base isolation story (see Fig. 2 and Photo 2), the elastic-plastic hysteretic damper is inserted into a complicated mechanism with tied two levers (see Fig. 3 and Photo 3). In Fig. 3, the deformable bar between two levers at the bottom has a

dimension of the cross-sectional depth $B = 1.68$ mm, the cross-sectional width $D = 1.67$ mm, the length $S = 5$ mm. These values have been determined from the initial stiffness and the equivalent damping ratio (the yield deformation is used as an intermediate parameter). An example of the load-displacement relation of the viscous damper under sinusoidal input is shown in Fig. 4 and that of the elastic-plastic hysteretic damper is presented in Fig. 5. In Fig. 4, the input frequency and stroke are 0.76 Hz and 10 mm, respectively. The input cycle is 100. On the other hand, in Fig. 5, the input frequency and stroke are 0.607 Hz and 20 mm, respectively. The input cycle is 200. In the experiment of hysteretic dampers, a large deformation in the base-isolation story occurs after the failure of hysteretic dampers. In order to limit the large deformation in the base-isolation story, a stopper (deformation limiting apparatus; also distance of two levers is 27 mm) has worked. This results in the large reaction in Fig. 5.

The capacity of both dampers is determined so that the dissipated energies are equivalent at a specified deformation (25 mm) (Jennings 1968). Fig. 6 shows the schematic diagram for defining the equivalent damping ratio for elastic-plastic hysteretic dampers. In Fig. 6, k_d = initial stiffness of hysteretic damper, k_s = post-yield stiffness of hysteretic damper, Q = intercept of damper force at
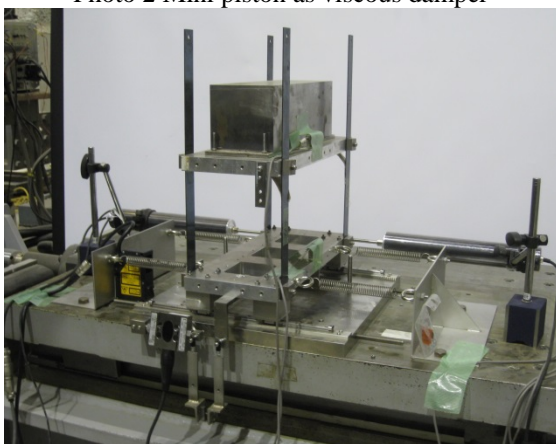

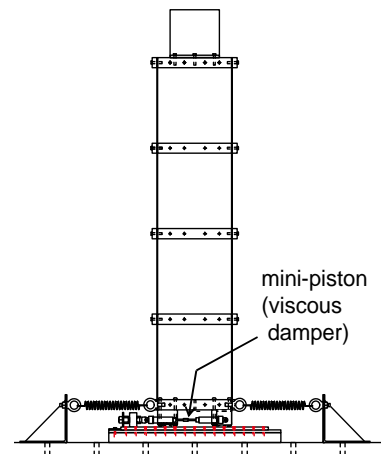Photo 2 Mini piston as viscous damper

Fig. 2 Viscous damper in base-isolated story

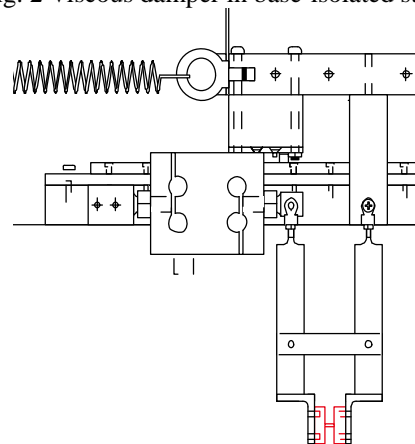
Photo 3 Elastic-plastic hysteretic damper

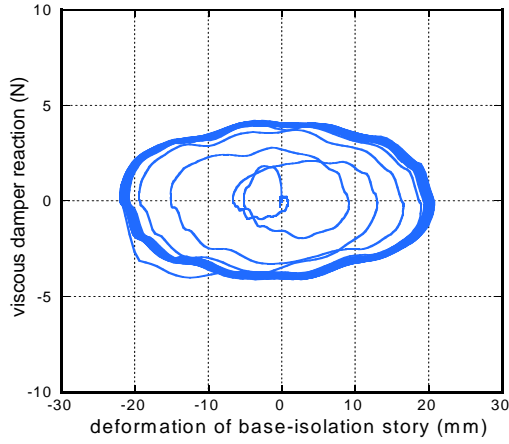Fig. 3 Elastic-plastic hysteretic damper

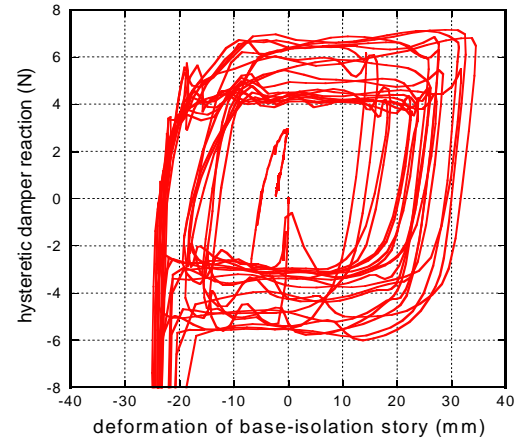Fig. 4 Load-deformation relation for viscous damper

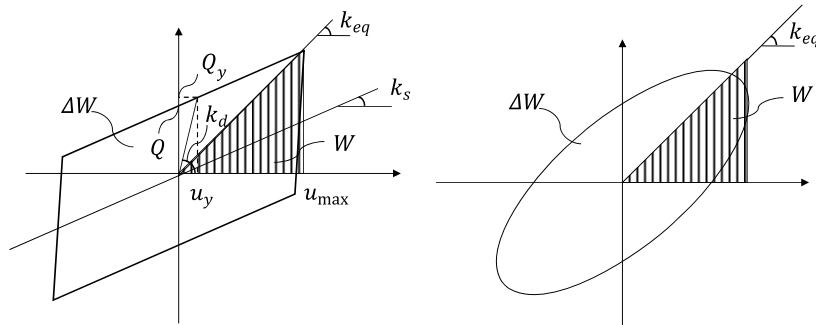Fig. 5 Load-deformation relation for elastic-plastic hysteretic damper

Fig. 6 Schematic diagram of equivalent damping ratio for hysteretic elastic-plastic dampers

zero deformation, Q_y=yield force of hysteretic damper, u_y=yield deformation of hysteretic damper, k_{eq}=equivalent stiffness of hysteretic damper, u_{max}=maximum deformation of hysteretic damper, W=elastically stored energy for equivalent system at the maximum deformation, ΔW =one-cycle dissipated energy of hysteretic damper. Then the equivalent viscous damping ratio, equivalent stiffness and equivalent damping coefficient may be expressed by

$$h_{eq} = \frac{1}{4\pi} \cdot \frac{\Delta w}{w} = \frac{2k_d u_y (u_{max} - u_y)}{\pi u_{max}(k_d u_y + k_s u_{max})}, \quad k_{eq} = k_s + \left\{ k_d (u_y / u_{max}) \right\}, \quad c_{eq} = \frac{4k_d u_y (u_{max} - u_y)}{\pi \omega_1 u_{max}^2}$$

where ω_1: fundamental natural circular frequency of the equivalent system.

3. Experimental results

A displacement-control sinusoidal base motion has been input from the shaking table as shown in Figs. 1 and 3 and Photo 1. In the shaking table test, a sinusoidal wave has been input. This is
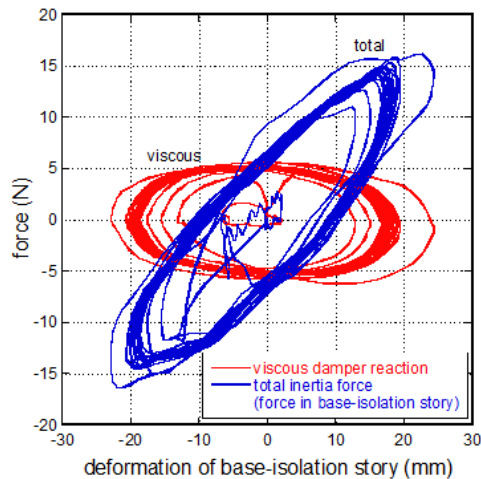
Fig. 7 Relation of total inertial force in model with a viscous damper with displacement in base-isolated story and reaction of viscous damper
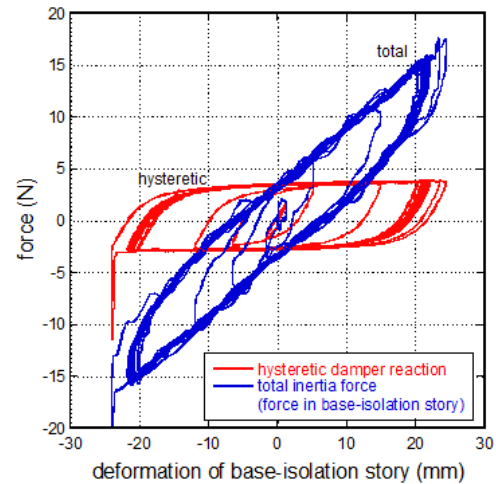
Fig. 8 Relation of total inertial force in model with a hysteretic damper with displacement in base-isolated story and reaction of hysteretic damper
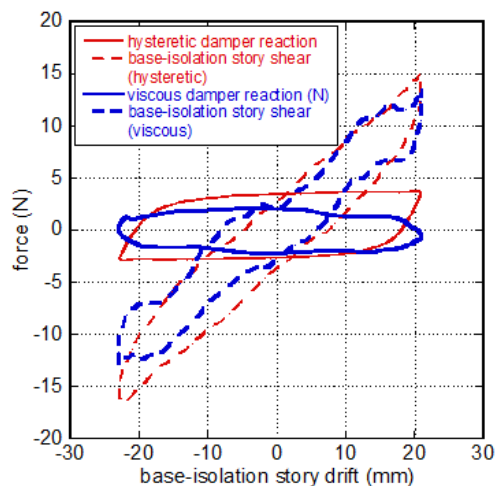
Fig. 9 Example loop 1 of total inertial force vs displacement in base-isolated story and reaction of dampers
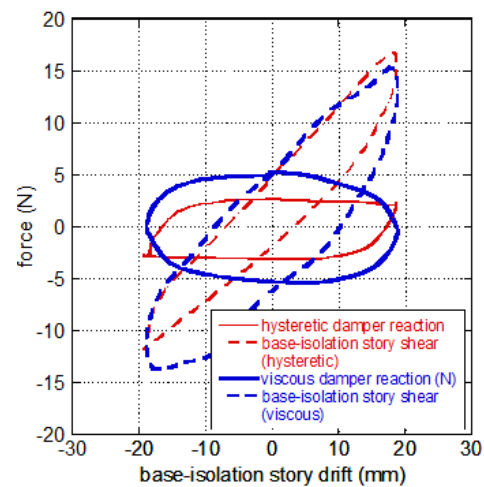
Fig. 10 Example loop 2 of total inertial force vs displacement in base-isolated story and reaction of dampers

because the present paper focuses on the resonant response of a base-isolated building with a long-period ground motion which can be modeled well by a sinusoidal wave. Fig. 7 shows the relation of the total inertial force (measured from the accelerometers on all the floors) in the model with a viscous damper with the displacement in the base-isolated story together with the relation of reaction in the viscous damper with the displacement in the base-isolated story. The input frequency and stroke are determined as 1.186 Hz and 20 mm, respectively. The input cycle is 20.

On the other hand, Fig. 8 presents those for the model with an elastic-plastic hysteretic damper. The input frequency and stroke are determined as 0.593 Hz and 16mm, respectively. The input cycle is 15. It is noted that the reaction in the elastic-plastic hysteretic damper measured by a load cell is also plotted in Fig. 8. For clarity, Figs. 9 and 10 show two examples of loop of the total inertial force vs. the displacement corresponding to Figs. 7 and 8. It can be observed that, while the shape of the relation of the total inertial force in the model with a viscous damper with the displacement in the base-isolated story exhibits a round one at the tip depending on the property of viscous dampers, that with an elastic-plastic hysteretic damper exhibits a sharp one depending on the property of elastic-plastic hysteretic dampers.

It may be concluded from Figs. 9 and 10 that the proposed experimental system can simulate approximately the responses of base-isolated buildings with viscous or elastic-plastic hysteretic dampers.

4. Bound of aspect ratio

4.1 Definition of bound of aspect ratio

The definition of bound of aspect ratio is shown in Fig. 11. The plan of the building is given as shown in Fig. 12 and the size and location of rubber bearings are also prescribed. Then the ratio of the building height to the building width is defined as the aspect ratio and its limiting value is found. The constraints on the following three design conditions are considered here.
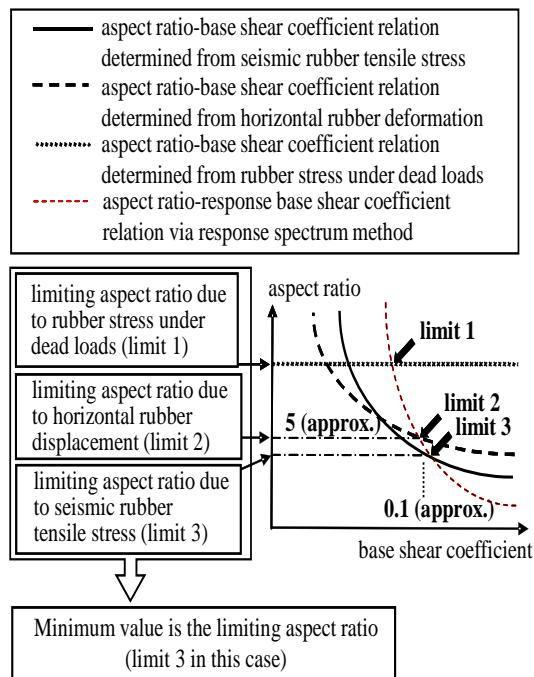

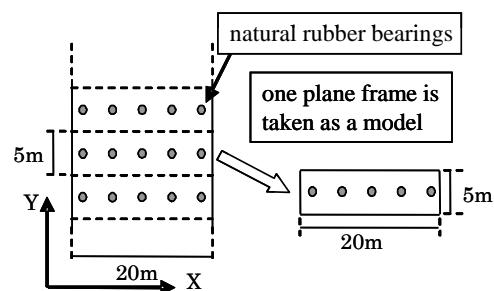Fig. 11 Definition of bound of aspect ratio
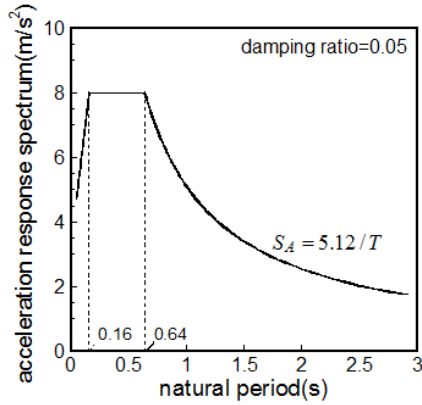

Fig. 12 Building plan

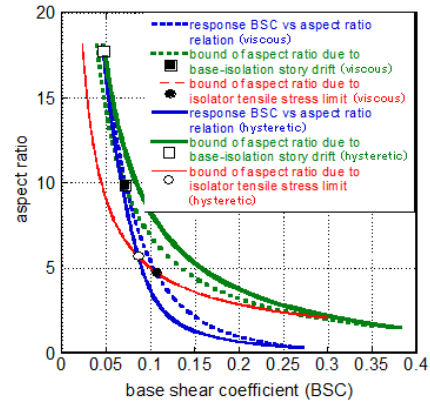Fig. 13 Acceleration response spectrum for large earthquakes used in Japan (2000)

Fig. 14 Relation of aspect ratio with base shear coefficient

(i) The design condition on the compressive stress of rubber bearings under dead loads

(ii) The design condition on the tensile stress of rubber bearings under dead loads and seismic disturbance (the limiting value of tensile stress is 0 N/mm^2)

(iii) The design condition on the shear deformation of rubber bearings under seismic disturbance

The constraint on axial compressive stress of rubber bearings under dead loads and seismic disturbance is assumed now to be satisfied. In fact, the control of the axial stress of rubber bearings under dead loads and the tensile stress of rubber bearings under seismic loading enables one to satisfy that constraint in a direct manner. If desired, this constraint can be added without difficulty.

The most direct method to obtain the bound of aspect ratio is to change the building height sequentially and evaluate the above-mentioned design conditions. When one of the design constraints is violated for the first time, that aspect ratio becomes the limiting value (bound). While this procedure is direct, the check of the design condition (ii) is elaborate. For this reason, the base shear coefficient is used as a key parameter in this paper and a simple analysis method proposed in the Reference (Hino *et al.* 2008) is utilized for analyzing axial deformation of base-isolation rubber bearings. An evaluation method proposed in the Reference (Hino *et al.* 2008) is also used simultaneously of the base shear coefficient under a design response spectrum.

4.2 Analysis of bound of aspect ratio

A single-degree-of-freedom model is used as a model for the seismic response evaluation and it is assumed that the deformation can be described approximately by the lowest-mode vibration component only. This assumption is well recognized in the structural design practice of base-isolated buildings. The acceleration response spectrum for large earthquakes used in Japan (Building Standard Law 2000) is employed (see Fig. 13). That acceleration response spectrum (in m/s^2) for damping ratio=0.05 can be expressed in terms of the natural period *T* by

$$S_A = 3.2 + 30T \ (T < 0.16s)$$
$$S_A = 8.0 \ (0.16s < T < 0.64s)$$
$$S_A = 5.12 / T \ (0.64s < T)$$

(1)

The acceleration response spectrum for damping ratio h is calculated by multiplying the coefficient $1.5/(1.0+10h)$ on the response spectrum for $h=0.05$. This response spectrum is similar to the well-known one proposed by Newmark and Hall (1982).

4.2.1 Design condition on tensile stress of rubber bearings

If the deformation of an N-story building can be described approximately by the lowest-mode only, the base shear and overturning moment at the base under a base acceleration input $\ddot{x}_g$ can be expressed in terms of the lowest-mode normal coordinate $q_0^{(1)}$.

$$Q = M_1\left(\ddot{q}_0^{(1)} + \ddot{x}_g\right) \tag{2}$$

$$M_{ov} = M_1 H_1\left(\ddot{q}_0^{(1)} + \ddot{x}_g\right) \tag{3}$$

where M_1 and H_1 are the equivalent mass and the equivalent height of the equivalent SDOF model described by

$$M_1 = \beta_1 \sum_{i=0}^{N}(m_i u_i^{(1)}), \; H_1 = \beta_1 \sum_{i=0}^{N}(m_i h_i u_i^{(1)})/M_1 \tag{4}$$

$u_i^{(1)}$ and β_1 are the lowest-mode horizontal displacement and the participation factor of the lowest mode and m_i, h_i are the i-th story mass and i-th story height. From Eqs. (2) and (3), the relation $M_{ov} = QH_1$ holds. The aspect ratio-base shear coefficient relation determined from the design condition on tensile stress of rubber bearings can then be obtained from this relation and the governing equation for the base mat (stress analysis of rubber bearings) (Hino et al. 2008). The limit value 0 N/mm^2 of tensile stress of rubber bearings is employed.

4.2.2 Design condition on horizontal deformation in the base-isolation story

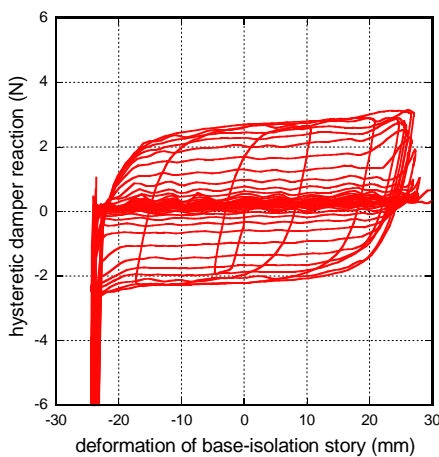If the base shear coefficient C_B is given, then the base shear can be expressed by

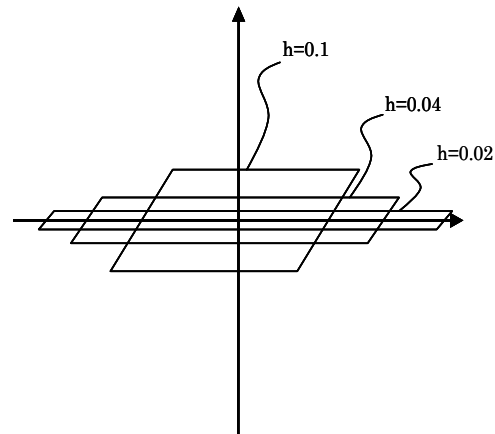Fig. 15 An example of load-displacement relation of present elastic-plastic hysteretic damper

Fig. 16 Simplified model of load- displacement relation in Fig. 15

$$Q = \left(\sum_{i=0}^{N} m_i \right) C_B g \tag{5}$$

where g is the acceleration of gravity. Eq. (2) can also be expressed as

$$Q = \beta_1 \left(\sum_{i=0}^{N} m_i u_i^{(1)} \right) \left(\ddot{q}_0^{(1)} + \ddot{x}_g \right) \tag{6}$$

Eqs. (5) and (6) provide

$$\ddot{q}_0^{(1)} + \ddot{x}_g = C_B g \left(\sum_{i=0}^{N} m_i \right) \bigg/ \left(\beta_1 \sum_{i=0}^{N} m_i u_i^{(1)} \right) \tag{7}$$

Let d denote the horizontal deformation in the base-isolation story. By keeping $\ddot{q}_0^{(1)} + \ddot{x}_g = \omega_1^2 q_0^{(1)}$, $d = \beta_1 u_0^{(1)} q_0^{(1)}$ in mind, d can be expressed as

$$d = u_0^{(1)} C_B g \left(\sum_{i=0}^{N} m_i \right) \bigg/ \left(\omega_1^2 \sum_{i=0}^{N} m_i u_i^{(1)} \right) \tag{8}$$

where g and ω_1 denote the gravitational acceleration and the fundamental natural circular frequency of the model. Eq. (8) provides the aspect ratio-base shear coefficient relation determined from the design condition on horizontal deformation in the base-isolation story.

4.2.3 Design condition on compressive stress under dead loads

This aspect ratio-base shear coefficient relation does not depend on the base shear coefficient and can be evaluated directly from the total weight of the building and foundation and the total cross-sectional area of rubber bearings.

4.2.4 Aspect ratio-response base shear coefficient relation

The building is designed based on the relation $T_1 = 0.02 H$ of the fundamental natural period T_1 (*s*) with the building height H (*m*). The fundamental mode of the building with a fixed base is assumed to be a straight line and the story stiffnesses are determined via an inverse problem formulation. Two models are used as the models for response spectrum method in order to evaluate the response base shear coefficient; one is a 2DOF model consisting of the SDOF building and the SDOF base-isolation system, the other is an SDOF model transforming the total system into a single-degree-of-freedom system. From this procedure, the aspect ratio-response base shear coefficient relation can be derived.

The intersection of this aspect ratio-response base shear coefficient relation with the active relation among three conditions explained above gives the limiting aspect ratio for the critical design condition (Hino *et al.* 2008).

5. Effect of change in physical properties of dampers on response during long-duration motion

It is well recognized that the properties of elastic-plastic hysteretic dampers deteriorate at the limit state. An example of the load-displacement relation of the present elastic-plastic hysteretic damper is shown in Fig. 15. This relation is modeled by a simplified one shown in Fig. 16. As explained in Fig. 5, in the experiment of hysteretic dampers, a large deformation in the base-isolation story occurs after the failure of hysteretic dampers. In order to limit the large deformation in the base-isolation story, a stopper (deformation limiting apparatus; also distance of two levers is 27 mm) has worked. This results in the large reaction in Fig. 15. But this phenomenon does not affect the damping deterioration process in Figs. 15 and 16. It is also assumed that the equivalent stiffness of the present elastic-plastic hysteretic damper becomes smaller towards the limit state. As for the property of viscous dampers, only a damping coefficient is assumed to become smaller due to the increase of temperature during strong shaking. The aspect ratio bounds are obtained by using the experimental results on the load-displacement relation (hysteresis loop) of the dampers and their simplified models in the analytical procedure. Since it seems difficult to incorporate the detailed deterioration process of hysteretic dampers, the bound of aspect ratio has been obtained for various damping ratios.

Fig. 17 shows the locus of the bound of aspect ratio for different damping ratios $h = (0, 0.02, 0.04, 0.06, 0.08, 0.10)$ for the model with a viscous damper. The diamond mark indicates the bound of aspect ratio due to base-isolation story drift limit and the square mark that due to isolator tensile stress limit. On the other hand, Fig. 18 presents the locus of the bound of aspect ratio for different damping ratios $h = (0, 0.02, 0.04, 0.06, 0.08, 0.10)$ for the model with an elastic-plastic hysteretic damper.

Fig. 19 illustrates the bound of aspect ratio with respect to the damping ratio of the model with a rigid super-structure. In this model, all the masses are concentrated to the bottom mass and the approximation of single-degree-of-freedom models has been employed. This experimental system
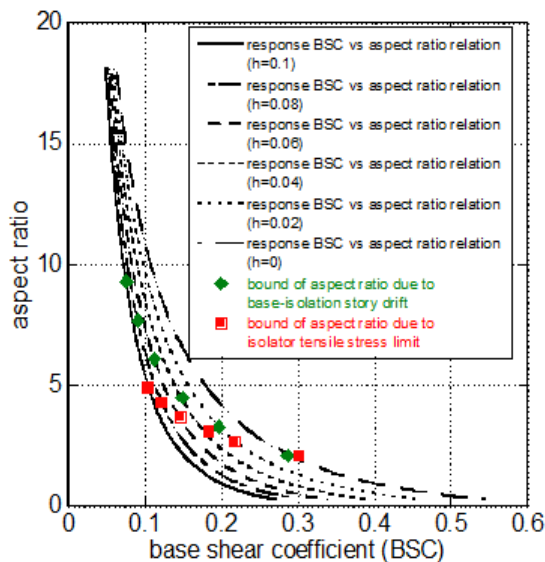

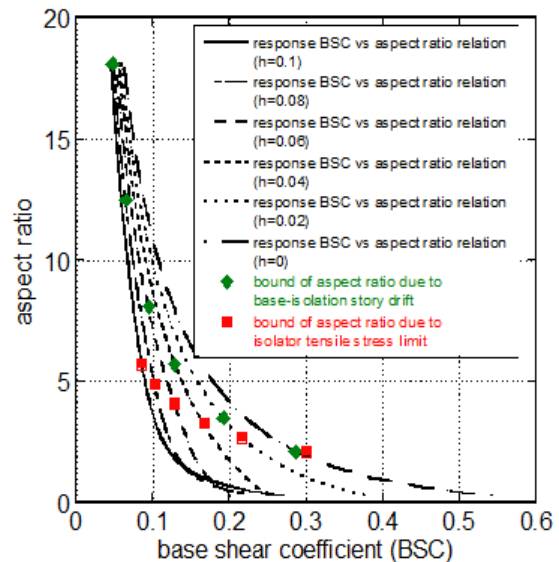Fig. 17 Locus of bound of aspect ratio for different damping ratios (viscous damper)

Fig. 18 Locus of bound of aspect ratio for different damping ratios (elastic-plastic hysteretic damper)
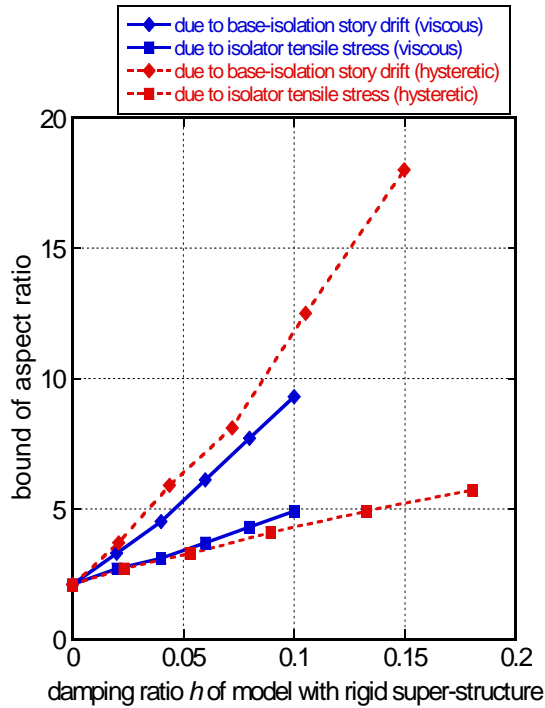
Fig. 19 Bound of aspect ratio with respect to damping ratio of model with rigid super-structure
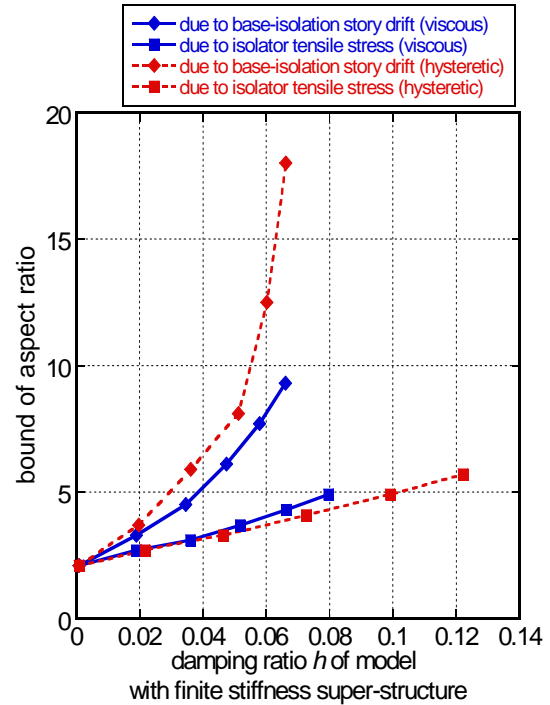
Fig. 20 Bound of aspect ratio with respect to damping ratio of total model with super-structure of finite stiffness

has been used to obtain the load-displacement relation (hysteresis loop) of the dampers and to demonstrate the resonant state of the base-isolated systems. It is not intended to derive the limit aspect ratio directly through the experiment. On the other hand, Fig. 20 presents the bound of aspect ratio with respect to the damping ratio of the total model with a super-structure of finite stiffness. In Fig. 20, both limits due to base-isolation story drift and isolator tensile stress are plotted. It can be observed from Fig. 20 that, when the capacity of both dampers is determined so that the dissipated energies are equivalent at a specified deformation, the bound of aspect ratio for the base-isolated structure with the elastic-plastic hysteretic damper is smaller than that with the viscous damper. This bound of aspect ratio is determined by the isolator tensile stress limit. This means that the base-isolated structure with the elastic-plastic hysteretic damper is more vulnerable than that with the viscous damper from this viewpoint.

6. Conclusions

The following conclusions have been obtained.

(1) The test structure on almost friction-free rails and supported by a mini piston or a low yield-point steel can be used as a test model of base-isolated building structures with a viscous damper or an elastic-plastic hysteretic damper.

(2) When the capacity of both dampers (a viscous damper or an elastic-plastic hysteretic damper) is determined so that the dissipated energies are equivalent at a specified deformation, it can be shown that the response of the base-isolated structure with the elastic-plastic hysteretic damper is larger than that with the viscous damper. This characteristic can also be demonstrated through the comparison of the bound of the aspect ratio. It has been shown that the bound of aspect ratio for the base-isolated structure with the elastic-plastic hysteretic damper is smaller than that with the viscous damper. This means that the base-isolated structure with the elastic-plastic hysteretic damper is more vulnerable than that with the viscous damper from this viewpoint.

(3) It has been demonstrated that, when the base-isolated structure is subjected to long-duration input, the mechanical property (especially damping ratio) of the elastic-plastic hysteretic damper deteriorates and the response of the base-isolated structure with that damper becomes larger than that with the viscous damper. This property has been confirmed through the comparison between the base-isolated structure with a viscous damper and that with an elastic-plastic hysteretic damper in terms of the bound of aspect ratio. It seems difficult to incorporate the process of deterioration of damper performance in the procedure of deriving the limit aspect ratio in detail. A more simple procedure of modeling of change of damping ratio for elastic-plastic hysteretic dampers has been used.

(4) The bound of aspect ratio plays a role as a measure of safety margin of tall base-isolated buildings. The introduction of a plot of the aspect ratio-base shear coefficient relation for a design condition together with the aspect ratio-response base shear coefficient relation under the design earthquake enables structural designers to understand the true safety margin in a unified manner.

Acknowledgements

References

Abrahamson, N., Ashford, S., Elgamal, A., Kramar, S., Seible, F. and Somerville, P. (1998), *Proc. of the First PEER Workshop on Characterization of Special Source Effects*, San Diego.

Ariga, T., Kanno, Y. and Takewaki, I. (2006), "Resonant behavior of base-isolated high-rise buildings under long-period ground motions", *Struct. Des. Tall Spec.*, **15**(3), 325-338.

Building Standard Law in Japan (2000).

Çelebi, M., Okawa, I., Kashima, T., Koyama, S. and Iiba, M. (2012), "Response of a tall building far from the epicenter of the 11 March 2011 M9.0 Great East Japan earthquake and aftershocks", *Struct. Des. Tall Spec.*, (published online).

Clemente, P. and Buffarini, G. (2010), "Base isolation: design and optimization criteria", *Int J. Seismic Isolation Protection Syst.*, **1**(1), 17-40.

Fujita, K. and Takewaki, I. (2011), "An efficient methodology for robustness evaluation by advanced interval analysis using updated second-order Taylor series expansion", *Eng. Struct.*, **33**(12), 3299-3310.

Hall, J.H., Heaton, T.H., Halling, M.W. and Wald, D.J. (1995), "Near-source ground motion and its effect on

flexible buildings", *Earthq. Spectra*, **11**, 569-605.

Heaton, T.H., Hall, J.H., Wald, D.J. and Halling, M.W. (1995), "Response of high-rise and base-isolated buildings in a hypothetical MW 7.0 Blind thrust earthquake", *Science*, **267**, 206-211.

Hijikata, K., Takahashi, M., Aoyagi, T. and Mashimo, M. (2012), "Behavior of a base-isolated building at Fukushima Dai-ichi nuclear power plant during the Great East Japan earthquake", *Proc. The Int. Sympo. Eng. Lessons Learned from the 2011 Great East Japan Earthq.*, March 1-4, 2012, Tokyo, Japan.

Hino, J., Yoshitomi, S., Tsuji, M. and Takewaki, I. (2008), "Bound of aspect ratio of base-isolated buildings considering nonlinear tensile behavior of rubber bearing", *Struct. Eng. & Mech.*, **30**(3), 351-368.

Jangid, R.S. and Banerji, P. (1998), "Effects of isolation damping on stochastic response of structures with nonlinear base isolators", *Earthq. Spectra.*, **14**, 95-114.

Jangid, R.S. and Kelly, J.M. (2001), "Base isolation for near-fault motions", *Earthq, Eng. Struct. Dyn.*, **30**, 691-707.

Jennings, P.C. (1968), "Equivalent viscous damping for yielding structures", *J. Eng. Mech. Div.- ASCE*, **94**(EM1), 103-116.

Kamae, K., Kawabe, H. and Irikura, K. (2004), "Strong ground motion prediction for huge subduction earthquakes using a characterized source model and several simulation techniques", *Proc. The 13th World Conference on Earthq. Eng.*, Vancouver.

Li, H.N. and Wu, X.X. (2006), "Limitations of height-to-width ratio for base-isolated buildings under earthquake", *Struct. Des. Tall Spec.*, **15**, 277-287.

Madden, G.J., Symans, M.D. and Wongprasert, N. (2002), "Experimental verification of seismic response of building frames with adaptive sliding base-isolation system", *J. Struct. Eng. - ASCE*, **128**(8), 1037-1045.

Mahmoud, S. and Jankowski, R. (2010), "Pounding-involved response of isolated and non-isolated buildings under earthquake excitation", *Earthq. Struct.*, **1**(2), 231-252.

Makris, N. and Chang, S.P. (2000), "Effect of viscous, viscoplastic, and friction damping in the response of seismically isolated structures", *Earthq. Eng. Struct. Dyn.* **29**, 85-107.

Minami, Y., Yoshitomi, S. and Takewaki, I. (2012), "System identification of super high-rise building using limited vibration data during the 2011 Tohoku (Japan) earthquake", *Struct. Cont. Health Monit.*, (Published online).

Naeim, F. and Kelly, J. (1999), *Design of seismic isolated structures*, John Wiley & Sons, New York.

Nakamura, Y., Hanzawa, T., Hasebe, M., Okada, K., Kaneko, M. and Saruta, M. (2011a), "Report on the effects of seismic isolation methods from the 2011 Tohoku–Pacific earthquake", *Int. J. Seismic Isolation Protection Syst.* **2**(1), 57-74.

Nakamura, Y., Saruta, M., Wada, A., Takeuchi, T., Hikone, S. and Takahashi, T. (2011b), "Development of the core-suspended isolation system", *Earthq. Eng. Struct. Dyn.* **40**, 429-447.

Nanda, R.P., Shrikhande, M. and Agarwal, P. (2012), Effect of ground motion characteristics on the pure friction isolation system", *Earthq. Struct.,* **3**(2), 169-180.

Newmark, N.M. and Hall, W.J. (1982), *Earthquake Spectra and Design*, Earthquake Engineering Research Institute, Berkeley, CA.

Olmos, B.A. and Roesset, J.M. (2010), "Effects of the nonlinear behavior of lead-rubber bearings on the seismic response of bridges", *Earthq. Struct.*, **1**(2), 215-230.

Sahasrabudhe, S. and Nagarajaiah, S. (2005), "Experimental study of sliding base-isolated buildings with magnetorheological dampers in near-fault earthquakes", *J. Struct. Eng. - ASCE*, **131**(7), 1025-1034.

Takewaki, I. (2008), "Robustness of base-isolated high-rise buildings under code-specified ground motions", *Struct. Des. Tall Spec.*, **17**(2), 257-271.

Takewaki, I. and Fujita, K. (2009), "Earthquake input energy to tall and base-isolated buildings in time and frequency dual domains", *Struct. Des. Tall Spec.*, **18**(6), 589-606.

Takewaki, I., Murakami, S., Fujita, K., Yoshitomi, S. and Tsuji, M. (2011), "The 2011 off the Pacific coast of Tohoku earthquake and response of high-rise buildings under long-period ground motions", *Soil Dyn. Earthq. Eng.*, **31**(11), 1511-1528.

Takewaki, I., Fujita, K. and Yoshitomi, S. (2013), "Uncertainties in long-period ground motion and its impact on building structural design: Case study of the 2011 Tohoku (Japan) earthquake", *Eng. Struct.*, **49**,

119-134.

Yamamoto, K., Fujita, K. and Takewaki, I. (2011), "Instantaneous earthquake input energy and sensitivity in base-isolated building", *Struct. Des. Tall Spec.*, **20**(6), 631-648.

Zhang, Y. and Iwan, W.D. (2002), "Protecting base-isolated structures from near-field ground motion by tuned interaction damper", *J. Eng. Mech. – ASCE*, **128**(3), 287-295.

CC